

## Crystallographic Texture Helps Reduce Hydrogen Induced Cracking in Pipeline Steels

V. Venegas, F. Caleyo\*, O. Herrera, J. Hernández-Sánchez and J. M. Hallen.

Departamento de Ingeniería Metalúrgica, IPN-ESIQIE, UPALM, Edif. 7, Zacatenco, México DF 07738, México.

\*E-mail: [fcaleyo@gmail.com](mailto:fcaleyo@gmail.com)

*Received:* 13 September 2013 / *Accepted:* 26 October 2013 / *Published:* 15 November 2013

---

Low-carbon steel samples, all within API specifications, were produced using different rolling/recrystallization schemes. These samples showed similar microstructure, but differed in their crystallographic textures. After cathodic hydrogen charging, HIC was detected in the cold- and hot-rolled/recrystallized steels, whereas the warm-rolled/recrystallized steels proved resistant to this damage. These results can be related to the differences in texture and grain boundary distribution observed in these groups of samples. It is concluded that it is feasible to improve the HIC resistance of pipeline steels through crystallographic texture control and grain boundary engineering. The use of warm rolling schedules has been proven an effective solution in achieving this goal as they lead to crystallographic texture dominated by the {111}ND-fiber texture, and to a high proportion of low-angle grain boundaries. These two characteristics are necessary to further reduce, beyond traditional methods, the susceptibility of pipeline steels to HIC.

---

**Keywords:** HIC, pipeline steel, crystallographic texture, warm rolling.

### 1. INTRODUCTION

The origin, mechanisms, and consequences of Hydrogen-induced cracking (HIC) have been documented over the last several decades [1]. The strategies to reduce the incidence of this damage have not proven to be totally effective for severe operating conditions [1,2], so that the control of crystallographic texture and grain-boundary distribution of sour-service steels has recently been proposed as a means to reduce their susceptibility to HIC [3].

In recent works the authors have shown that, at a grain scale, crystallographic texture and grain-boundary character can play a significant role in HIC propagation in pipeline steels [4–6]. From the results of these studies it was postulated that the resistance of low-carbon steels to HIC could be

improved by controlling their local texture and grain-boundary distribution [7]. Controlled warm-rolling, in the 600–800°C range, was proposed as a mean to produce crystallographic textures suitable for reducing HIC because of (i) a reduction in the number of transgranular and intergranular cleavage paths along {001}ND-oriented<sup>1</sup> grains, (ii) a reduction in crack coalescence and stepwise HIC propagation, and (iii) an increase in the number of high-resistance, intergranular crack paths along coincidence site lattice and low-angle grain boundaries between {111}ND-oriented grains.

New experimental evidence is presented in this work, which supports the hypothesis that the resistance of pipeline steels to HIC can be improved at a macroscopic scale through controlled warm rolling.

Several samples of pipeline steel, all within API 5L specifications [7], were obtained through different thermo-mechanical processes. These samples, all with similar microstructures, developed different crystallographic textures and grain-boundary statistics. Cathodic hydrogen charging was used to investigate their HIC behavior. The results of this study show that a strong {111}ND fiber texture, which results from warm rolling, reduces the HIC damage in sour-service pipeline steels.

## 2. EXPERIMENTAL DETAILS

A section of a new 610-mm (24-inch) API 5L X52 pipe was used to obtain RD-oriented strips in order to have identical starting samples of this steel (Table I). These samples were subjected to different thermomechanical treatments and a total of 5 usable samples, that is, with similar microstructures but different crystallographic textures, were selected for further testing. HIC tests were conducted by cathodic hydrogen charging for 48 hours in a hydrogen sulfide (H<sub>2</sub>S) saturated solution under a current density of 50 mA/cm<sup>2</sup>. The solution was selected very close to the TM 0177-B solution recommended in the NACE TM0284-96 standard [11].

**Table 1.** Chemical composition, in wt%, of the starting API 5L X52 steel

C	Mn	S	P	Si	Cu	Cr
0.212	1.334	0.032	0.028	0.037	0.021	0.009

Table 2 shows the thermomechanical paths followed by the investigated samples, which can be grouped into two categories: warm-rolled samples (WR1, WR2), and cold- and hot-rolled samples (HR1, HR2, CR1). All samples were first austenitized at 1040°C for 1 hour, then rolled as indicated in Table 2, and finally treated at 850°C for about 100 seconds to ensure complete recrystallization with no substantial grain growth.

The global or macrotecture X-ray texture of the samples was determined by measuring three incomplete pole figures: {110}, {200}, and {111} using a Mo texture goniometer. The orientation

<sup>1</sup> ND, RD, and TD refer to the pipe's Normal (radial), Rolling (axial), and Transverse (hoop) directions, respectively. {hkl}ND refers to a grain orientation for which the {hkl} plane lies parallel to the ND-TD plane.

distribution function (ODF) of each sample was determined from the measured pole figures assuming a cubic-triclinic symmetry. The ADC method [8] was used to estimated the ODFs, which are represented here in the  $\varphi_2 = 45$  deg. section of Euler space [9].

**Table 2.** Thermomechanical path followed by the investigated samples

Sample	Thickness reduction (%)	Path	Final rolling temperature (°C)
WR1	75	2 steps, 50% each	800
WR2	75	2 steps, 50% each	600
HR1	75	2 steps, 50% each	1040
HR2	50	15 steps, 5% each	1000
CR1	50	15steps, 5% each	27

The metallographic inspection and microtexture<sup>2</sup> study of the samples were performed using scanning electron microscopy and automated FEG/EBSD, respectively. Orientation Imaging Microscopy (OIM) was used to analyze the EBSD measurements. Grain boundaries (GBs) were defined in the EBSD-derived orientations maps by the presence of a point-to-point misorientation greater than 3 degrees. To study the mesotexture<sup>3</sup> of the samples, GBs were categorized into: (i) low-angle (LABs, with misorientation angles less than 15 deg.), (ii) high-angle (HABs), and (iii) coincidence site lattice (CSL,  $\Sigma n$  [9]).

### 3. RESULTS

Figure 1 shows examples of typical optical micrographs taken from the studied samples. It is observed the characteristic banded pearlite/ferrite microstructure of low-strength carbon steels after rolling and recrystallization [10]. The average grain size was found to be similar in all samples: 10  $\mu\text{m}$  for the warm-rolled samples and 12  $\mu\text{m}$  for the cold- and hot-rolled samples.

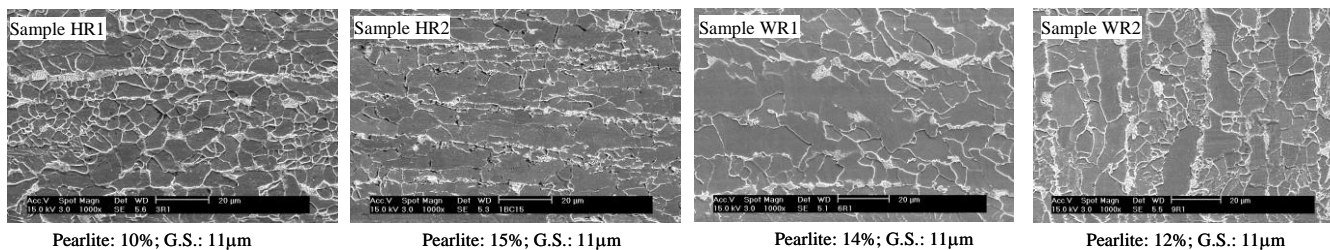


**Figure 1.** Optical micrographs of some of the investigated samples (G.S.: grain size).

<sup>2</sup> The term ‘microtexture’ refers to individual orientation measurements that can be related to their location in the sample. [9].

<sup>3</sup> ‘Mesotexture’ refers to the distribution, or texture, of GBs [9].

After cathodic hydrogen charging, the cold- and hot-rolled samples developed HIC, with cracks growing following intergranular and transgranular paths as shown in Fig. 2. In a remarkable contrast, no HIC damage was observed in any of the warm-rolled samples. It is important to stress that, given that cathodic hydrogen charging introduces more diffusible hydrogen into the steel than the standard HIC test (NACE TM0284-96, [11]), the present results are expected to be similar to those obtained had the latter method been used.

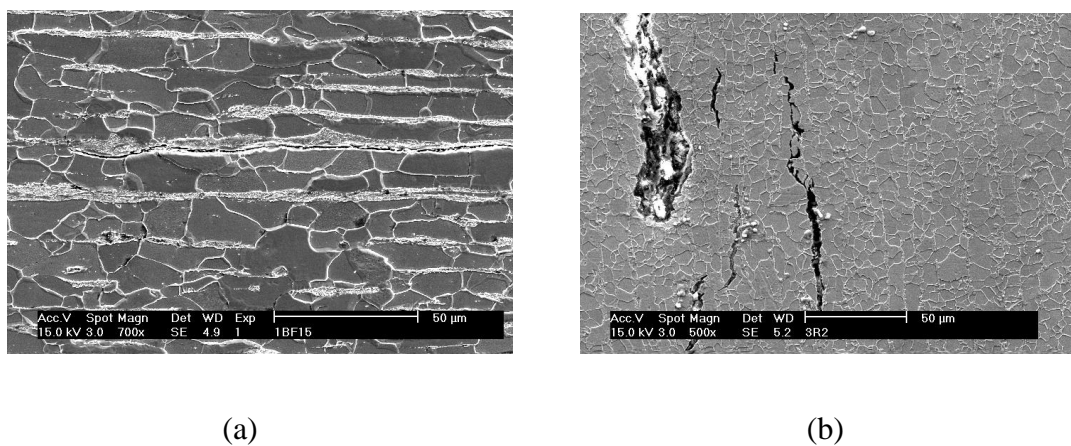


**Figure 2.** SEM micrograph of typical HIC-damaged regions in samples CR1 (a) and HR1 (b).

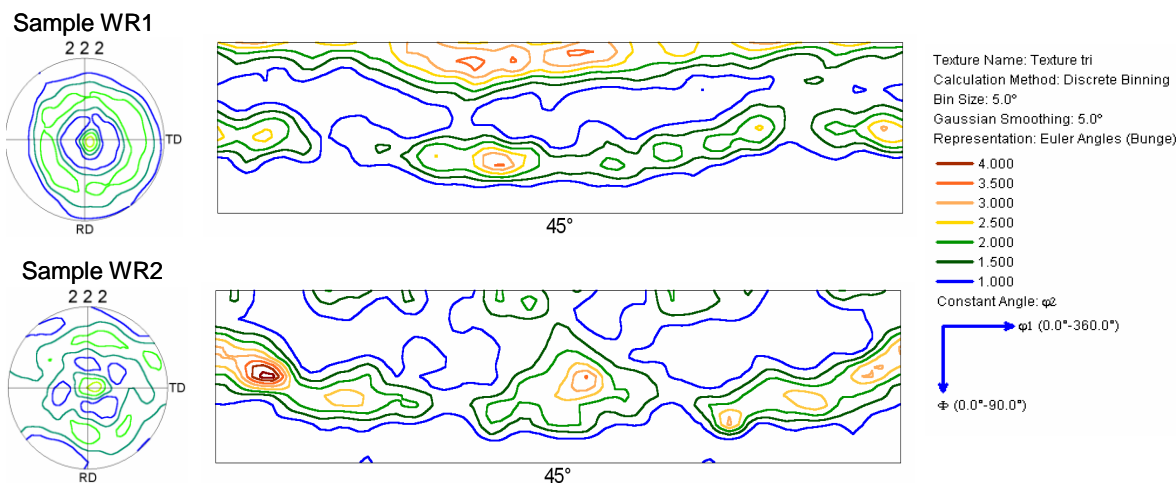


**Figure 3.** EBSD-derived {111} pole figure and  $\phi_2 = 45$  deg. section of the ODF in Euler space for the HIC-free group of samples.

For the group of HIC-free (warm-rolled) samples, whose pole figures and ODFs are shown in Fig. 3, the crystallographic texture is far from that of a random polycrystalline sample, with a low random (phon) texture component [8]. Based on the position of ideal orientations and texture fibre typical of rolled and recrystallized bcc steels [9], one realizes that sample WR1 has a well-developed

fiber texture, which is very close to  $\{111\}$ ND. Similarly, sample WR2 shows a strong  $\{111\}$ ND fiber, together with a much less noticeable, yet present,  $\{001\}$ ND fiber.

For the group of HIC-stricken samples, whose pole figures and ODFs are shown in Fig. 4, the crystallographic texture is markedly different from those found in the warm-rolled samples. Samples HR1 and CR1 show a much more isotropic texture, while sample HR2 shows a very acute texture, completely dominated by the  $\{001\}\langle 110\rangle$  component. In addition, the strength of the  $\{111\}$ ND and  $\{112\}$ ND fibers in these three samples is much less sharp than in the warm-rolled ones. In sample HR1, for example, the  $\{111\}$ ND fiber seems to dominate the texture. However, when compared with samples WR1 and WR2, the sharpness of this texture fiber is significantly less in HR1. Furthermore, the texture phon or true random component of this sample was found to be 35%, which denotes that its texture has a significant random character.

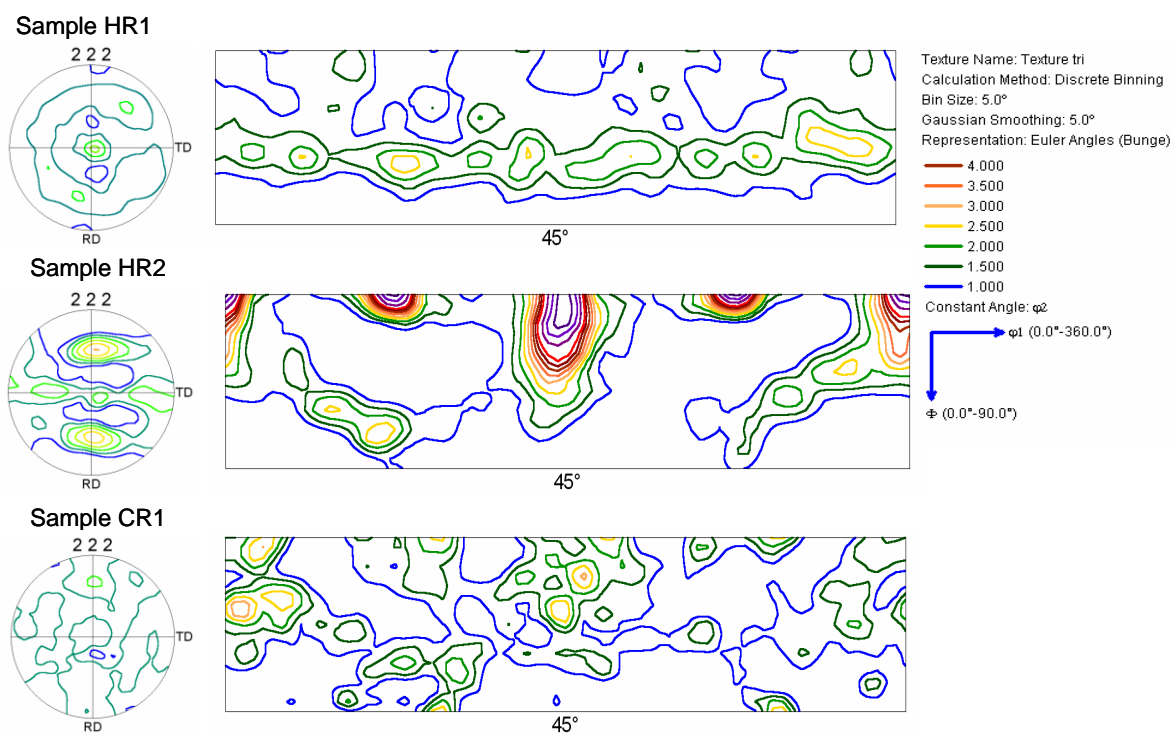


**Figure 4.** EBSD-derived  $\{111\}$  pole figure and  $\varphi_2 = 45$  deg. section of the ODF in Euler space for the HIC-stricken group of samples.

The results of the metallographic inspection and crystallographic texture analysis were corroborated by the EBSD/OIM studies. The orientation (OIM) maps derived from the EBSD measurements showed no evidence of texture heterogeneities such as orientation clustering or correlation. The microstructural and texture characteristics estimated from these maps, such as grain size and pole figures and ODFs, agree with the results previously found during the metallographic

inspection and texture analysis of the studied samples.<sup>4</sup> Based on these findings, and on the fact that the number of grains in the orientation maps of the test samples is relatively large (of the order of, or greater than 10<sup>4</sup>), one can be concluded that the local EBSD-derived distribution of GBs is representative of that of the bulk sample. Figure 5 shows the grain boundary statistics or mesotexture in the HIC-free and HIC-stricken groups of samples. The first result to stress from the results in Fig. 5a is that the proportion of CSL boundaries observed for these two groups of samples is not statistically significant. Therefore, in Fig. 5b, where the average proportion of HABs and LABs are shown for both groups of samples, CSLs boundaries are accounted for as HABs.

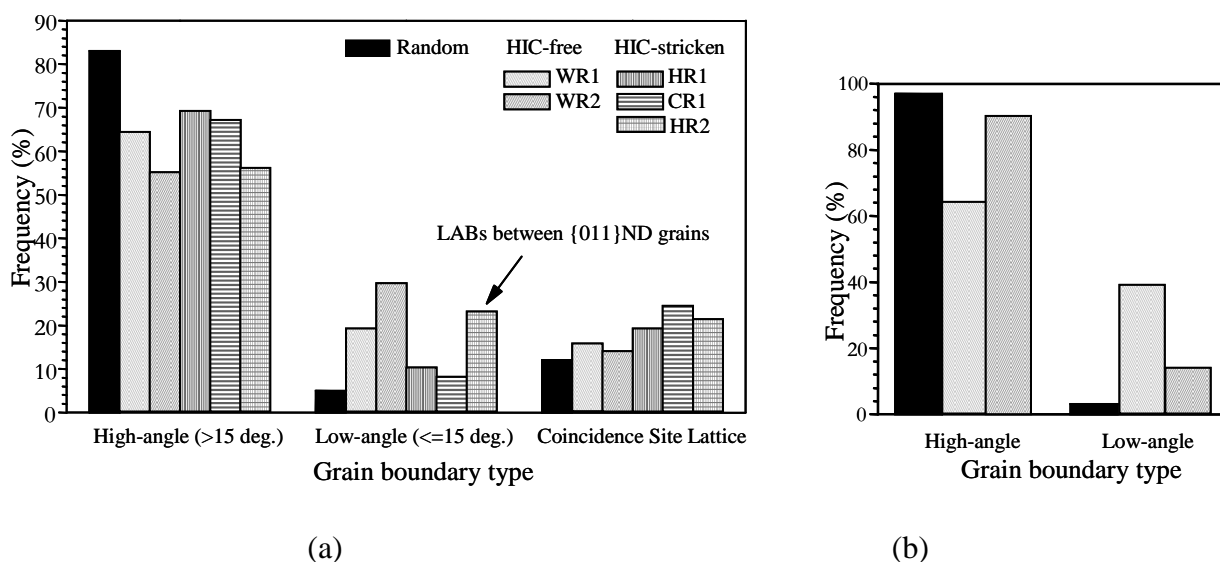


**Figure 5.** Mesotexture of the investigated samples. (a) By sample, considering with CSLs separately accounted for. (b) By group of samples with CSLs accounted for as high-angle boundaries.

For the group of HIC-free (warm-rolled) samples the GB statistics shows the highest proportion of low-angle boundaries and departs considerably from that of the (theoretically-deduced) random polycrystal. This result is in complete agreement with the results shown in Fig. 3 for the crystallographic texture of these samples, and is an indication that no significant orientation correlation [12] occurs in them. Similarly, orientation correlation was also neglected for the group of HIC-stricken samples. Fig. 5b also shows that, on average, the fraction of LABs in the HIC-free group of samples almost doubles that of the HIC-stricken group. In contrast, the proportion of HABs in the HIC-free group is about 45% lower than in the HIC-stricken group.

For the group of HIC-stricken samples (except for HR2) the mesotexture is the closest to that of the random polycrystal. The fraction of LABs in samples HR1 and HR2, on average, close to 13%; this proportion is about half of that observed for the rest of the test samples. In a very particular case, sample HR2 shows a remarkably higher fraction of LABs. However, given the results shown in Fig. 4,

<sup>4</sup> Given this result, and for the sake of space economy, the pole figures and ODF presented in this paper are those obtained from the EBSD measurements

and under the assumption of absence of orientation correlation, it is reasonable to expect that the majority of these GBs occurs between grains with orientations close to  $\{001\}$ ND. The implications of this for HIC propagation is discussed later. Samples HR1 and CR1 show a high fraction of HABs, which, on average, is about 45% higher than the proportion observed in the HIC-free samples. Once again, sample HR2 stands out as a remarkable exception, where the small fraction of HABs and CSLs can be related to the high fraction of LABs shared by  $\{001\}$ ND-oriented grains.

#### 4. DISCUSSION

In the group of samples where HIC was observed, the absence of a strong  $\{111\}$ ND texture fiber and the proximity of the texture to that of the random polycrystal is critical to the results of the HIC tests. In this group, HR2 is the only sample whose texture significantly differs from that of the random polycrystal. The sharpness of the texture of this sample can be unambiguously related to the observed dominant proportion of  $\{001\}$ ND-oriented grains. The observed susceptibility of these samples to HIC can be associated with their grain mesotexture, which results from the texture that they develop during deformation and recrystallization. The relatively large proportion of high-angle GBs observed in samples HR1 and CR1 provide plentiful of low-resistance paths for the propagation of intergranular HIC. Sample HR2 shows a significantly increased fraction of low-angle GBs, but between grains with orientations close to  $\{001\}$ ND (Fig. 4).

The large number of  $\{001\}$ ND grains observed in sample HR2 reduces the resistance of this sample to HIC as it facilitates intragranular crack propagation along  $\{001\}$  cleavage planes oriented parallel to the pipe's rolling plane. In addition, LABs shared by  $\{001\}$ ND also provide low-resistance paths to intergranular, cleavage-like propagation of HIC in the same plane [5,6,12].

In a remarkable contrast, the warm-rolled, HIC-free samples show a crystallographic texture dominated by well-developed, strong  $\{111\}$ ND or  $\{112\}$ ND texture fibers. In reference [7] it was shown that, at a grain scale, these orientations impede transgranular HIC propagation on the rolling plane. One can also point out that, for a mode I loading, shear stress is null ahead of crack tips [13]; therefore, propagation of HIC in the rolling plane by shear/slip-related fracture along grains with orientation within these fibers can be predicted to be very unlikely. Another characteristic of grains with  $\{111\}$ ND orientations is that they can accumulate large plastic deformation when cracks are close enough to induce interaction and coalescence. This improves the resistance of the steel to HIC by reducing the driving force for growth of interacting cracks, with the consequent reduction in the probability of coalescence of closely-spaced, non-coplanar cracks [13,14].

In addition to the foregoing, the warm-rolled group of samples is particularly prone to have improved HIC resistance because it exhibits an increased number of LABs between  $\{111\}$ ND-oriented grains. It has been reported [7] that LABs with  $\langle 111 \rangle$  disorientation axis have lower energies than LABs with  $\langle 100 \rangle$  axis. As a result, a steel with a strong  $\{111\}$ ND texture is expected to show a reduced susceptibility to HIC due to the increased presence of low-angle boundaries with the lowest possible energy.

## 5. CONCLUSIONS

It has been shown that it is feasible to improve the HIC resistance of pipeline steels using crystallography texture control and grain-boundary engineering. At a macroscopic scale, this can be achieved through controlled warm (ferritic) rolling schedules. These thermomechanical processes lead to a crystallographic texture dominated by the {111}ND-fiber texture and to a mesotexture with a high proportion of low-angle, low-energy grain boundaries. These two characteristics are critical to reduce, beyond traditional practices, the susceptibility of these steels to hydrogen-induced cracking.

## ACKNOWLEDGMENTS

The comments and suggestions made by the reviewers are greatly appreciated.

## References

1. Review of Published Literature on Wet H<sub>2</sub>S cracking of Steels Through 1989, 2003 Edition, NACE International Publication 8X294, Houston TX, 2003.
2. C.R.F. Azevedo, *Eng. Failure Anal.* 14 (2007) 978.
3. M.A. Al-Anezi, S. Rao, *J. Failure Anal. Preven.*, 11 (2011) 385.
4. V. Venegas, F. Caleyó, J.L. González, T. Baudin, J.M. Hallen, R. Penelle, *Scr. Mater.*, 52 (2005) 147.
5. V. Venegas, F. Caleyó, J.M. Hallen, T. Baudin, R. Penelle, *Metall. Mater. Trans.*, A 38 (2007) 1022.
6. V. Venegas, F. Caleyó, T. Baudin, J. M. Hallen, R. Penelle, *Corros. Sci.*, 51 (2009) 1140.
7. V. Venegas, F. Caleyó, T. Baudin, J.H. Espina-Hernández, J.M. Hallen, *Corr. Sci.*, 53 (2011) 4204.
8. K. Pawlick, *Phys. Status Sol. B*, B134 (1986) 477.
9. V. Randle and O. Engler. Introduction to Texture Analysis. Macrotecture, Microtexture and Orientation Mapping, Francis & Taylor, London, 2003.
10. R.K. Ray, J.J. Jonas, *Int. Mater. Reviews*, (1990) 35, 1.
11. NACE Standard Test Method TM0284-96, Evaluation of Pipeline and Pressure Vessel Steels for Resistance to HIC, NACE, Houston, (1997) pp. 1–10.
12. M.A. Arafin, J.A. Szpunar, *Corros. Sci.*, 51 (2009) 119.
13. Y.Z. Wang, J.D. Atkinson, R. Akid, and R.N. Parkins, *Fatigue Fract. Eng. Mater. Struct.*, 19 (1996) 427.
14. F. Erdogan and G.C. Sih, *J. Basic Eng.*, 85 (1963) 519.